Menopause-associated proteomic and lipidomic alterations in high-density lipoprotein: Perimenopause is characterized by smaller triacylglycerols-enriched particles.

Satu Lehti[1], Tia-Marje Korhonen[1], Rabah Soliymani[2], Hanna Ruhanen[3,4], Emilia Lähteenmäki[5], Mari Palviainen[6], Pia Siljander[6], Maciej Lalowski[2,7], Reijo Käkelä[3,4], Maarit Lehti[5] Eija K Laakkonen[1]*

[1]Gerontology Research Center and Faculty of Sport and Health Sciences, University of Jyväskylä, Jyväskylä, Finland

[2]Meilahti Clinical Proteomics Core Facility, Helsinki Institute of Life Science (HiLIFE), and Faculty of Medicine, University of Helsinki, Helsinki, Finland

[3]Helsinki University Lipidomics Unit (HiLIPID), HiLIFE, and Biocenter Finland, University of Helsinki, Helsinki, Finland

[4]Molecular and Integrative Biosciences Research Program, Faculty of Biological and Environmental Sciences, University of Helsinki, Helsinki, Finland

[5]Faculty of Sport and Health Sciences, University of Jyväskylä, Jyväskylä, Finland

[6]Extracellular vesicles (EV) group and EV core, Molecular and Integrative Biosciences Research Programme, Faculty of Biological and Environmental Sciences, University of Helsinki, Helsinki, Finland

[7]Institute of Molecular Biology and Biochemistry, Department of Gene Expression, Faculty of Biology, Adam Mickiewicz University, Poznań, Poland

Abstract

Menopause is associated with a proatherogenic shift in serum metabolome and high-density lipoprotein (HDL) particle size distribution. We analyzed lipidomes and proteomes of HDL with nuclear magnetic resonance and mass spectrometry from pre-, peri-, and postmenopausal women to get a deeper insight into the structure of HDL. The S-HDL particles constituted 62% of all HDL particles in perimenopause and 60% in pre- and postmenopause, thus, perimenopausal HDL had the highest S-HDL lipid content, notably, being enriched in triacylglycerols. This feature is a known risk factor for coronary heart disease. We identified 728 proteins from the purified HDL particles and quantified 44 representing functional classes of lipid metabolism, transport and signaling, immune defense, and regulation of cellular processes. Perimenopausal HDL exhibited fewer apolipoproteins (APOA1, APOA2, APOC1, APOC3, and APOE) per particle than premenopausal. We did not detect menopausal status-associated deteriorations in the LCAT activity or cholesterol efflux capacity, albeit the calculated lipid class ratios suggest defects, especially within PERI XL-HDL particles, potentially affecting the particle size distribution and triacylglycerol content. In summary, menopause is associated with structural differences in HDL potentially compromising the cardioprotective quality of HDL.

Introduction

Serum lipid metabolome changes with age and during menopause towards the proatherogenic direction[1–3]. The high-density lipoprotein cholesterol (HDL-C), an indicator of "better atherogenic health", tends to rise from premenopause to postmenopause concomitant to the reduced cardioprotective ability of HDL particles[4,5]. This contradiction may be explained by compositional changes, which lead to functional deficits as particle size distribution shifts towards smaller

diameters[1,3] while reverse cholesterol transport has been shown to increase across the menopausal transition resulting in a net decrease in cholesterol efflux capacity per HDL particle[4].

In circulation, HDL particles form a heterogeneous population, varying from small discoidal ones to larger spherical particles (sizes 7-12 nm)[6]. In addition to a variety of lipids[7], HDL particles contain a versatile mixture of proteins[8], the most abundant being apolipoprotein APOA1. This compositional heterogeneity allows HDL particles to also display great functional variety. HDL particles have, for instance, been found to modulate functions of innate immunity, glucose metabolism, and cellular communication[9–11]. HDL core lipid composition is modified by enzymes such as cholesteryl ester transfer protein (CETP)[12] and lecithin:cholesterol acyltransferase (LCAT)[13], which are considered to define the anti-atherogenic potential of HDL.

In this study, we investigated HDL lipidome and proteome using nuclear magnetic resonance (NMR) and mass spectrometry to characterize molecular differences in HDL particles between pre-, peri-, and postmenopausal women. The lipid and protein profiles of perimenopausal women's HDL stand out from the profiles of pre- and postmenopausal women. We hypothesize that the high hormonal fluctuations during perimenopause may alter the composition and thereby functional profiles of HDL particles leading to functionally less atheroprotective particles than in premenopause.

Results

To assess the compositional differences and functional properties of HDL between menopausal statuses, we selected 216 healthy, non-medicated normolipidemic women aged 47–56 years from the Estrogenic Regulation of Muscle Apoptosis (ERMA) cohort[14] to represent premenopause (PRE), perimenopause (PERI) and postmenopause (POST) statuses. Menopausal status was determined by hormone measurements and self-reported menstrual diaries. To minimize within-group variation among individuals and to obtain sufficient serum sample volume allowing HDL purification, six individual serum samples were combined into a pool, and 12 such pools per menopausal stage were used in the analysis (Fig. 1). Characteristics of the three menopause groups are presented at group means level in Table 1 and as pooled sample level in supplemental Table 1. Menopausal groups were otherwise similar except that women in the POST group were about two years older and had lower estradiol and sex hormone-binding globulin and higher follicle-stimulating hormone (FSH) levels demonstrating that the menopause had occurred. In addition, the clinical measures of total cholesterol, low-density lipoprotein cholesterol (LDL-C), and HDL-C were the highest, and glucose was the lowest in the POST group.

Figure 1

Table 1

Physical characteristics of pre-, peri- and postmenopausal HDL

The total concentration of HDL particles, concentrations of S, M, L, and XL sized HDL particles, and the lipid concentrations of the particles were profiled using an NMR metabolomics platform[15]. The mean HDL particle size (Fig. 2a, PRE - PERI $p = 0.014$, PERI - POST $p = 0.029$), the mean HDL particle concentration in serum (Fig 2b, PERI - POST $p = 0.0006$), and the mean HDL total lipid content (Fig. 2d, PRE - PERI $p = 0.023$, PERI – POST $p = 0.0006$) were the lowest in PERI group. Next, we inspected the different HDL particle size groups. The S-HDL particles constituted 62.3% of all particles in PERI, and 59.6% and 59.9% in PRE and POST, respectively (Fig. 2c). Consequently, in the PERI group the S-HDL lipid content was higher (Fig. 2e, PRE - PERI $p = 0.015$, PERI - POST $p = 0.030$), while in the L-HDL

the lipid content was lower (PRE - PERI p = 0.024, PERI - POST p = 0.038) than in PRE or POST groups. In M- and XL-HDL the lipid content was similar in all menopausal statuses.

Figure 2

Proportions of major lipid classes in the HDL particle size groups

The overall lipid content of the HDL particles was assessed by NMR to measure the molar amounts of lipids belonging to four major lipid classes triacylglycerols (TG), unesterified cholesterols (FC), phospholipids (PL), and cholesteryl esters (CE). We found statistically significant differences between the PERI and POST groups in the HDL content of all lipid classes (Fig. 3), while the PRE and POST groups resembled each other. Notably, the PERI group had the highest proportion of TGs, especially in the S-HDL particles (Fig. 3a). This tendency has earlier been shown to be associated with coronary heart disease[16]. Subtle differences between the PERI and POST groups were also observed in the proportions of FCs (lower in PERI than POST), PLs (higher in PERI than POST), and CEs (lower in PERI than POST). By inspecting the HDL particle size groups (Fig. 3b), we were able to identify the main sources of these observations to M-HDL, which presented less FC in the PERI than POST (p=0.003) and XL-HDL with more FC in the PERI than POST (p=0.011). The source of the observed differences between the PERI and POST groups in PLs was localized to M-HDL (p=0.006). We could not identify the source of the group difference observed between PERI and POST groups in total CE content (Fig. 3d).

Figure 3

Characterization of serum extracellular vesicles as a potential source of bias for the ultracentrifugally isolated HDL

For more detailed HDL lipidomic and proteomic analyses, we isolated HDL particles from the pooled serum samples with sequential ultracentrifugation (Fig. 1). However, it is known that thusly separated HDL-containing fraction of serum (d<1.21 g/ml) may also contain extracellular vesicles (EVs) and proteinous complexes[17,18]. To evaluate if the PRE, PERI, and POST groups differed in their EV content, which thereby could form a significant source of bias to our HDL-omics results, we used size exclusion chromatography (SEC) to isolate EVs from the aliquot of the same pooled serum samples later used for HDL-omics. The isolated EVs were characterized using the ExoView technology with anti-CD41, -CD9, -CD63, and -CD81 staining. The size of EVs was similar in all menopausal groups and there were no statistical differences in the PRE, PERI and POST groups regarding the typical tetraspanins CD81 and CD63 (Supplementary Fig. 1). However, there was a statistically significant difference between the PRE and POST groups regarding EV markers relevant for platelet-derived EVs (CD41 and CD9, p = 0.002 and 0.013, respectively), suggesting that the POST serum samples had reduced levels of platelet EVs compared to PRE group. However, neither group differed from the PERI group. We consider that EV-derived lipids and proteins will form only a negligible number of hits compared to more numerous HDL-derived hits[19].

HDL lipidomics: lipid species and fatty acids

As presented in Fig. 1, after HDL isolation, the HDL lipids were extracted, and lipid species were analyzed with electrospray ionization-mass spectrometry (ESI-MS). From the total lipid extract, fatty acids (FA) were derivatized into fatty acyl methyl esters (FAME) and analyzed with gas chromatography using flame ionization and mass-selective detectors (GC-FID and GC-MS, respectively).

Of all lipid species, we included for the main analysis only species that had a relative concentration over 0.5 mol-%, and for each lipid class, we present the six most abundant lipid species in Supplementary Fig. 2. In all menopausal statuses, the most abundant CE-species was CE 18:2, accounting for over 64 mol-% of all CEs. The most abundant phosphatidylcholine (PC) was PC 34:2, which accounted for about 24 mol-% of all PC-species. Lysophosphatidylcholines (LPC) LPC 18:2 and LPC 16:0 together accounted for over 50 mol-% of all LPCs. Sphingomyelins (SM) SM 34:1;O2 and SM 42:2;O2 together accounted for 47 mol-% of the SMs. The most abundant TG was TG 50:1 with about 20 mol-% portions among all TGs. The lipid species with significant group differences are presented in Fig. 4. Statistical significance was reached for CE 18:3 (PRE - POST $p = 0.004$, PRE - PERI $p = 0.014$), LPC 18:0 (PRE - PERI $p = 0.025$), LPC 22:6 (PRE - POST $p = 0.049$) and PC 38:6 (PRE - POST $p = 0.040$), TG 50:0 (PERI - POST $p = 0.034$) and TG 54:3 (PERI - POST $p = 0.015$).

For FA analysis, species with relative concentrations above 0.1 mol-% were included. The highest mol-% of odd chain FAs 15:0, 17:0 *anteiso* (a branched chain FA), and 17:0 ($p = 0.008$, $p < 0.001$ and $p = 0.018$, respectively) were observed in the PRE, medium values in the PERI and the lowest relative concentrations in the POST group, leading to significant group differences between the PRE and PERI statuses (Supplementary Fig. 3a). The opposite trend was observed for n-6 polyunsaturated FAs pathway with lowest relative concentration in the PRE and the highest in POST group, although of them, only the intermediary FA 18:3n-6 differed significantly between the groups (p= 0.022), while more abundant precursor FA 18:2n-6 and the downstream product FA 20:4n-6 did not reach statistical significance (Supplementary Fig. 3b).

HDL proteomics

Proteomic analysis utilizing liquid chromatography-tandem mass spectrometry (LC-MS) was carried out on ultracentrifugally isolated HDL particles (Fig. 1). Of the total 728 proteins detected, 44 proteins were quantified utilizing the robust criteria of being present in at least two out of three technical replicates and simultaneously in two out of twelve samples per menopausal group. The quantified HDL proteins were further annotated by their positioning concerning their known functions within Gene Ontology (GO) molecular function or biological processes terms in four major functional classes including lipid metabolism, transport and signaling, immune defense, and regulation of cellular processes (Fig. 5 and Supplementary Table 2).

Figure 5

Since we observed differences in HDL particle counts between the menopausal groups (Fig. 2), we present here the HDL proteins normalized to NMR-derived HDL particle counts (Fig. 6). The unnormalized data are presented in Supplementary Fig. 4. HDL particles can contain multiple copies of APOA1, with up to five copies in the largest particles[20]. Therefore, we also calculated the protein abundances normalized to LC-MS-measured APOA1 (Supplementary Fig. 5). Interestingly, 75% (34 of 45) of proteins (HDL particle count normalized) exhibited the highest or the lowest relative amount in the PERI compared to PRE or POST stages, although not all differences were statistically significant (Fig. 6).

Figure 6

The most abundant apolipoproteins in our data were APOA1, APOAC3, APOA2, APOD, APOC1, APOC2, and APOE. Of them, APOA1 and APOA2 are the main structural apolipoproteins of HDL. All these apolipoproteins exhibited the lowest abundance in the PERI samples even when the lower number of the HDL particles in the PERI group was considered (Fig. 6). Ratio of APOA2 to APOA1 and

the ratio APOA2 to HDL particle counts were the lowest in the PERI samples, suggesting that either there were fewer APOA2 proteins in each HDL particle or less APOA2-containing HDL particles.

Other proteins than apolipoproteins also showed statistically significant differences between the menopausal statuses. Among proteins assigned with transport-related functions, including HDL binding protein (HDLBP, also known as vigilin), phospholipid transfer protein (PLTP), carnitine O-palmitoyltransferase 2 (CPT2), metal transporter (CNNM4), and exportin-7 (XPO7), all except XPO7, exhibited the lowest relative abundancies in the PERI group (Fig. 6). Of the proteins classified with immune defense or cellular regulatory functions, significant group differences with lowest relative abundance in the PERI group were observed for mitochondrial amidoxime reducing component 2 (MTARC2), type I cytoskeletal keratin 9 (KRT9), tetratricopeptide repeat protein 37 (TTC37), adenylate kinase isoenzyme 1 (AK1), PITH domain containing 1 (PITHD1), dipeptidyl peptidase 2 (DPP7), proteasome maturation protein (POMP) and ornithine aminotransferase (OAT). Only small nuclear ribonucleoprotein D2 polypeptide (SNRPD2) had the highest relative abundance in the PERI group (Fig. 6). While the relative abundance of serum amyloid A-4 (SAA4), a constitutively translated apolipoprotein linked to inflammatory diseases, was higher in the PERI compared to the PRE and POST groups based on both normalization methods, the statistically significant difference between the PRE and PERI groups was reached only with APOA1 normalized SAA4 ($p = 0.015$).

Multi-omics integration analyses

Next, we used partial least squares discriminant analysis (PLS-DA) to inspect if a complete omics class or their combination instead of a single item would differentiate menopausal statuses from each other. PLS-DA of the lipids (main lipid classes together, one lipid class at the time or separate FAs), pinpointed the separation of the POST group while the PRE and PERI clusters mostly overlapped (Fig. 7a). The separation of the POST group was especially clear with all the main lipid classes or with SM only. When PLS-DA was applied to PC and LPC, samples of the PERI group scattered across the plot, while in the CE plot, the PERI samples clustered more tightly together than the other groups. In the PLS-DA of the proteins, however, the separation of all menopause groups was more pronounced than in the lipid analyses. The correlation circle in Fig. 7b shows two big clusters on the opposite sides of the circle indicating a strong negative correlation between members of these two clusters, while within each cluster the correlation is positive[21]. The left-side cluster included, e.g., mitochondrial proteins OAT and MTARC2 and apolipoproteins APOA2, APOA4, and APOC2. TGs with mid-length and low saturation level FAs correlated positively with the protein cluster, while longer chain highly unsaturated TGs correlated negatively. In the heatmap presented in Fig. 7c, the PERI samples tended to cluster together, while the PRE and POST samples appeared intermingled (rows), and lipids and proteins formed separate clusters (columns). Interestingly, many of the left-side cluster proteins of the circle plot were also included among the protein cluster of the heatmap, thereby strongly contributing to the separation of the PERI samples from the other menopausal groups.

Figure 7

Functional characterization of HDL within menopausal groups

We took several approaches to gain insight into whether menopause-associated differences in the HDL composition could manifest as functional differences. First, we calculated lipid class ratios, which can be used as indicators of the functionality of HDL particles. The activity of the HDL core lipid composition modifying enzyme LCAT can be estimated using ratios FC/PL and FC/CE (higher LCAT activity leads to lower ratios) whereas a higher TG/CE ratio reflects higher CETP activity[22,23]. Ratios were calculated using the NMR data, and thereby are presented as total HDL and HDL size

group-specific values. TG/CE ratio (Fig. 8a) was highest in the PERI group when calculated from the total HDL (PERI - POST $p = 0.049$) and remained at the highest level in the PERI among the menopausal groups when calculation was done per HDL size groups, although the ratio differed significantly only in XL-HDL between the PERI and POST groups (p=0.048). The group differences in mean values for FC/PL (Fig. 8b) and FC/CE (Fig. 8c) were very small. The PERI group had the lowest FC/PL value in total HDL (PERI - POST $p = 0.030$) and in M-HDL (PERI - POST $p = 0.002$) but the highest in XL-HDL (PRE - PERI $p = 0.013$). The ratio FC/CE differed significantly only for XL-HDL where PERI had a higher value than PRE ($p = 0.040$) and POST ($p = 0.007$). FC content of HDL is partly regulated by LCAT[24], thus these results suggest that LCAT might not act optimally with the XL-HDL particles and the regulation of the particle size and TG content is compromised.

Second, we assessed if the differences in lipid ratios in the pooled serum samples could be linked to actual differences in serum LCAT activity in individual samples from the different menopausal groups. Therefore, we measured the LCAT activity of ten PRE, nine PERI, and nine POST women. To avoid whole-body adiposity-related differences, every participant's BMI was matched with each other and the pooled BMI of the menopausal groups. The mean BMI was 25 ± 0.3 kg/m^2. We did not observe differences in the measured LCAT activity between the groups (Fig. 8d). LCAT activity, however, was found to correlate negatively ($r = -0.475$, $p = 0.011$) with serum estradiol concentration. Interestingly, the correlation was not linear at the low estradiol range; the women with low estradiol concentration, mainly representing the POST group, had a high variation with LCAT activity, but not in estradiol concentration.

Third, to find out if the menopausal status is associated with differences in the cholesterol efflux capacity of the HDL, we measured the ability of the isolated HDL from the different menopausal groups to take up fluorescently labelled cholesterol from THP-1-monocyte-derived macrophages. Although a slight increase in the efflux capacity was observed across advancing menopausal status, no statistical significance between the groups was detected (Fig. 8e).

Fourth, since we observed differences in certain FAs (Supplementary Fig. 3), we also examined if FA synthesis pathway functions differ in menopausal statuses. Therefore, we calculated Δ6, Δ5, and total desaturase potentials[25] (Fig. 8f), but found no significant differences between menopausal groups.

Figure 8

Discussion

In this study, we analyzed HDL from women representing three menopausal statuses to investigate menopause-associated differences in the HDL particle characteristics (size, lipidome, and proteome). After menopause, the risk of atherosclerotic cardiovascular diseases (ACVD) increases, despite that the measured HDL-C remains high. That prompted us to study the quality of HDL as the potential underlying cause for menopause-associated increase in ACVD incidences. Our multi-omics approach provided evidence for the perimenopausal period to be a critical transition stage in HDL properties. It appeared that perimenopausal women deviated from the pre- and postmenopausal women regarding HDL particle size distribution and lipid content although, on specific lipid species, some differences were also observed between pre- and postmenopausal women. The PERI group stood out also regarding HDL proteomics but in this case, it deviated more from the PRE rather than the POST group.

In our cross-sectional study, we observed that, in many of the studied variables, the perimenopausal state exhibited the expected less favourable HDL-associated profile compared to premenopause.

However, rather unexpectedly we noticed that the negative trends of HDL properties did not seem to deteriorate further in the postmenopausal group, but instead often reversed approaching levels of the premenopausal status. For example, we identified a smaller mean particle diameter, which is a proatherogenic feature compared to antiatherogenic larger particles, in the PERI group compared to PRE, but the mean particle size was again larger in the POST group compared to PERI. One plausible explanation for this phenomenon could be that we selected our study participants to be overall cardiometabolically healthy and not needing pertinent medications, hence our sample does not completely represent the average postmenopausal population with higher health variations. Consequently, the negative trends associated with menopause may be the most pronounced only in the group undergoing the strongest hormonal fluctuations. Therefore, our study only partially repeats the findings from earlier longitudinal studies showing that the circulating HDL particle pool tends to shift towards smaller and potentially more proatherogenic size distribution during menopausal transitioning[1,3,4].

The size of the HDL particles is not only an important indicator of lipid transport efficiency, but it also defines particle curvature thereby affecting particle cargo as well as the affinity of particles to vascular arterial intima and proteoglycans[26]. Some proteins prefer smaller HDL particles, while others prefer larger ones. For example, small apolipoproteins are not as evenly distributed as APOA1 but are found only in some HDL particles[27]. As the HDL particle size largely dictates the composition of HDL proteome and the proportions of lipid classes and species within a particle, it may also determine the functional properties of HDL in different menopausal statuses. For instance, low PL and high TG contents of HDL are associated with cardiovascular diseases[7,28]. Estrogen replacement therapy for postmenopausal women increases HDL particle size and changes the PL composition of HDL towards a more atheroprotective direction[29,30]. In our study, total PL and TG proportions were the highest in perimenopausal women, although group differences in proportions of PL were small and the finding was not completely congruent, since the opposite was observed in the XL-HDL particles in the PERI group. Nevertheless, as a net sum of these findings, we suggest that unstable estradiol levels may increase the risk of cardiovascular diseases in perimenopausal women.

Further insight into the HDL functional properties can be gained by inspecting the lipid ratios, which can indirectly reveal the efficiency of different lipid-associated enzymes. Since TG is trafficked between HDL and other circulating lipoproteins by CETP in exchange with CE, high CETP activity can lead to low HDL CE and high HDL TG[31,32] resulting in a higher TG/CE ratio as was found here in the PERI compared to other menopausal groups. The TG-rich HDL becomes a substrate of hepatic lipase and the concomitant CETP-mediated CE transfer from HDL to other lipoproteins reduces the size of HDL particles[33]. TG enrichment and higher TG/CE ratio have been shown to promote greater cholesterol efflux from macrophages into HDL particles simultaneously deteriorating LCAT efficiency and cholesterol disposal from the HDL particles[34,35]. Since LCAT esterifies FC to CE, it greatly affects HDL's ability to deplete FC from cells[36]. The situation is further complicated because HDL particles are also carriers of estrogens, which affects their cholesterol efflux capacity. The efflux capacity was enhanced in premenopausal HDL and in male HDL particles loaded with estradiol fatty acyl esters compared to male HDL lacking estrogen esters[37]. Although we did not detect significant differences in cholesterol efflux between the menopausal groups, our results somewhat agree with previous findings. The higher FC/PL, FC/CE, and TG/CE ratios especially in the largest XL-HDL particles of the PERI group indicate lower LCAT activity[38] and higher CETP activity[22] pointing towards less functional HDL. The functionality of HDL particles and the activity of LCAT and CETP are also affected by the apolipoprotein composition of the particles[39] as will be discussed together with other HDL proteomic findings.

Studies on menopausal differences in the HDL lipid species or fatty acid composition are scant, thus our findings in this respect are novel. We found differences in the relative concentrations of six lipid species and four fatty acids between the menopausal groups. The previous study from Tabassum *et al.*[40] investigated age and sex differences in serum lipid species and also included exploratory analyses of menopausal status, but the lipid species they pinpointed did not overlap with our findings. Relating to our findings, serum levels of CE 18:3 (we observed the highest molar percentage in postmenopausal HDL), and LPC 18:0 (we observed the lowest molar percentage in premenopausal HDL) have been associated with increased cardiovascular disease risk[41] while PC 38:6 and LPC 22:6 (we observed the lowest relative concentration in postmenopausal HDL for both) have been linked to a lowered risk of cardiovascular mortality[42]. Regarding FAs, we mostly observed menopausal differences with decreasing trends from pre- to postmenopause in the odd-chain FAs of HDL, which may be diet-derived or results of gut microbiota metabolism[43,44]. We also observed one even-chain FA, FA 18:3n-6 (gamma-linolenic acid), synthesized by one desaturation step from a diet-derived FA18:2n-6 (linoleic acid), to be significantly highest in postmenopause. FA18:3n-6 can be used as a precursor of arachidonic acid FA20:4n-6, which is, in turn, a precursor of eicosanoids including platelet-made blood clotting agent thromboxane, and is linked with systemic inflammation and elevated blood pressure[45]. HDL lipidome has been shown to respond to changes in diet[46], thus it is tempting to assume that the differences we observed could also be attributed to differences in diet. However, the diet information available to us is a rather coarse diet quality score, thus it was impossible to reveal differences in the quality of the diet among women in the menopausal groups.

APOA1 and APOA2 are the most abundant with the ability to be included in multiple copies in each particle[47]. Their levels have been shown to be estrogen-responsive; increasing with postmenopausal administration of estrogen therapy and rapidly decreasing after its cessation[50]. Therefore, it was not a surprise to observe lower levels of APOA1 and APOA2 in the HDL from peri- and postmenopausal women compared to premenopausal women. These estrogen-associated differences in APOA1 and APOA2 levels may have functional consequences for HDL particles. APOA1 activates LCAT, in turn, APOA2 and other apolipoproteins either inhibit or activate LCAT depending on the availability of APOA1[50], thus the number of APOA1 proteins per HDL particle affects reverse cholesterol transport efficiency. Furthermore, APOA2/APOA1 ratio has also been found to indicate the stability of HDL particles as APOA2 prevents APOA1 dissociation from HDL particles[51,52].

Altogether we were able to quantify 14 apolipoproteins of the APOA-, APOC- and APOE-families. Apart from APOA1 and APOA2, others are exchangeable and present only in a fraction of all HDL particles in circulation. The observed high HDL TG proportions and low APOC1 levels in perimenopausal women concur with studies where the low abundance of APOC1, an inhibitor of lipoprotein lipase and CETP in normolipidemic human subjects, increases plasma TG levels and TG enrichment to HDL[53,54]. We also observed the lowest APOC3 and APOE levels in perimenopause. Both have been found to be inversely correlated with estrogen levels[48,49], therefore it is puzzling that the lowest abundance was not found in premenopausal women with the highest estrogen concentrations. APOE modulates receptor-mediated HDL particle clearance[51]. High APOC3 levels have been linked with susceptibility to cardiovascular diseases as TG levels are positively associated with APOC3 levels[55]. An intricate interplay between APOC3 and APOE with the cholesterol efflux capacity has been observed; CETP was enriched in APOE-containing particles while LCAT was most abundant in HDL particles lacking APOC3, APOE, or both[39].

APOE is also involved with immune defense mechanisms[56]. In mice, it has been shown to decrease inflammatory molecules on endothelial cells, thereby reducing lipid accumulation in vascular endothelium[57]. In contrast to anti-inflammatory APOE, another HDL protein, SAA4 is linked to

dysfunctional HDL inducing low-grade inflammation[58] and deep vein thrombosis[59]. SAA isoforms can replace APOA1 from HDL particles thereby influencing particle structure and function[60]. We observed the highest relative amounts of SAA4 in the PERI group, but only when the protein levels were normalized to APOA1, suggesting that in perimenopausal women part of the APOA1 may have been replaced with SAA4. The low level of APOE concomitant with high SAA4 may hence indicate the decreased anti-inflammatory capacity of HDL particles especially in a perimenopausal state.

Hypothetically, the many changes in protein composition in different menopausal statuses may synergize with the more subtle lipid changes and together they may affect the HDL functionality. The single lipid class-level analysis was not efficient in separating menopausal groups, but the hypothesis was supported by the results from our PLS-DA analysis of HDL-multi-omics. A group of potentially interconnecting HDL-proteins including mainly apolipoproteins and mitochondrial proteins was positively correlated with low saturation level TGs and negatively with highly unsaturated TGs with longer chain FAs. In a heatmap allowing menopausal group-based visualization, the separation of proteins and lipids pinpointed the differing relative expression levels in the PERI group (lower levels for most of the proteins and some lipids and higher levels for most of the lipids) compared to the samples from PRE and POST groups.

We acknowledge that our study has some limitations. Firstly, this study is an observational study on healthy relatively normolipidemic Caucasian white women without known metabolic diseases or medications, thus, our results may not be directly generalizable for women representing other ethnic backgrounds or women with different levels of obesity, metabolic syndrome, or otherwise unhealthier conditions. However, to our knowledge, this is the first multi-omics attempt to characterize HDL composition in well-defined menopausal groups, and as such, it has merits albeit being a hypothesis-generating rather than a full mechanism-revealing study. Secondly, we did not analyze individual samples, but rather pooled serum samples representing altogether 126 individuals. This was a deliberate choice taken for practical reasons: The HDL isolation protocol is manually laborious and needs a substantial amount of serum for all the designated analyses. Pooling samples decreases the individual variation, which allowed a smaller number of samples per group to be used. This may, alas, also hide some individual findings and mask outliers by causing regression to mean. Thirdly, HDL particles can be isolated with many different methods each providing compositionally and functionally slightly different HDL particle pools[61]. Here, we chose the most common method that has been available since the 50's, the density gradient ultracentrifugation. We are aware that HDL may shed proteins during ultracentrifugation, and thus the protein content may not be comprehensive. We also found some traces of APOB and LPA despite using the two-step sequential ultracentrifugation method, which first separates APOB-containing lipoprotein particles followed by separation of the APOA1-containing particles. APOB, referring to APOB-100 protein, is integral part of Lp(a)-particles with density similar to HDL, thus it is not uncommon to identify these traces HDL proteomics as also reported by Holtzer et al[61]. In their comparative study of three different HDL particle isolation methods, they found all methods to result in the same contaminants or co-eluents. Interestingly, their further investigation by SEC as a second purification step indicated that APOB and LPA were mainly found in the fraction containing >12 nm particles, which might indicate that they derive from larger protein complexes. Therefore, we consider APOB and LPA as co-eluting contaminants rather than HDL-associated protein. Due to practical reasons, we were not able to apply the SEC as a second purification step for our HDL isolates. However, as EVs are known to enrich in the same ultracentrifugation fraction with HDL[18], we also inspected the EV content of the same pooled serum used for the HDL isolations. Taken that the concentration of EVs has been considered negligible when the HDL properties are described[18,19] and that no differences were found in CD81 and CD63 positive EVs distribution, although some differences were found in the CD41 and

CD9 positive EVs between PRE and POST groups, we consider that the input of EVs on our results is minor. Fourth, the questionnaire that the participants filled out in the ERMA study did not contain comprehensive food diaries, hence the dairy/fish/red meat consumption was not available for this study.

In summary, we conducted an extensive analysis of HDL particle composition in menopausal women, encompassing size distribution, lipidomics (including main lipid classes, lipid species, and fatty acids), and proteomics. Our findings reveal distinct differences in HDL among women in different menopausal stages, with interestingly perimenopause, not postmenopause standing out from the premenopause. Notably, perimenopausal women exhibit several summative differences in HDL, particularly in physical characteristics, lipid class and protein content and functionality suggesting a compromised anti-atherogenic capacity. This opens a new focus on the perimenopausal phase as a period of change, which may be relevant for the worsened cardiovascular health. This warrants further studies, especially to determine whether these observed differences are reversible traits specific to the perimenopausal state with hormonal fluctuations or if they signify structure-to-function deficits precipitating poor cardiovascular health into later postmenopausal stages.

Methods

This study uses serum samples from The Estrogenic Regulation of Muscle Apoptosis (ERMA) study[14]. The study was conducted according to the declaration of Helsinki. All participants provided informed written consent and the study was approved by the Ethical Committee of the Central Finland Health Care District (8U/2014). Among 1393 women who came to the first blood sampling session and had their menopausal status defined based on menstrual diaries and FSH measurements[14], we selected 216 representative healthy participants (72 women for each menopausal group) with strict exclusion criteria to allow forming 12 serum sample pools representing each pre-, peri- and postmenopausal statuses. Each pool was constructed from a 1.2 ml serum of six study participants and thereafter aliquoted and stored at -80 °C as three fractions later used for NMR, EV inspections, and HDL purifications.

Exclusion criteria for the current study included cancer, inflammatory diseases (asthma, rheumatoid arthritis, iritis, allergies, celiac disease, psoriasis, rosacea, flu-like symptoms, gastrointestinal disorders), metabolic disorders (diabetes mellitus types 1 and 2, elevated blood pressure, or disorders of lipid metabolism), any cardiovascular diseases, use of hormonal contraceptives or menopausal hormone therapy, statins, and cortisone. In addition, participants with missing information on diseases or BMI were not included.

Leisure-time physical activity and overall quality of the diet were assessed with structured questionnaires as in Karppinen *et al.* 2022[3]. The physical activity volume is expressed as metabolic equivalent hours per day (MET-h/d), which accounts for the duration, frequency, and intensity of leisure-time physical activity and the time spent on active commuting. The diet quality was assessed as a sum score computed based on the participant's responses to a 45-item food-frequency questionnaire. The higher score reflects a healthier diet. BMI was calculated as body mass per height squared (kg/m^2).

Blood sampling and serum analysis

Venous blood samples were drawn from the antecubital vein in the supine position, after overnight fasting between 7 and 10 a.m. in Vacuette® CAT Serum Clot Activator tubes (Greiner Bio-One GmbH, Austria). After a 30-minute incubation at room temperature to allow clotting, the samples were centrifuged at 2200 × g for 10 min at RT. The obtained serum was aliquoted and stored at −80 °C

until analysis. Cortisol, insulin, estradiol, sex hormone-binding globulin, and FSH concentrations of serum were determined using IMMULITE 2000 XPi (Siemens Healthcare Diagnostics, UK). Glucose, cholesterol, LDL-C, HDL-C, and TG concentrations were determined using a Konelab 20XTi analyzer (Thermo Fisher Scientific, Finland).

Nuclear magnetic resonance spectroscopy

The first fraction (0.5 ml) of the pooled serum samples was used to analyze lipoproteins and metabolites with a targeted proton nuclear magnetic resonance (1H-NMR) spectroscopy platform (Nightingale Health Ltd, Finland; biomarker quantification version 2020). The technical details of the method have been reported previously[62].

Extracellular vesicle characterization

The second fraction (0.6 ml) of pooled serum samples was used to assess EVs. EVs were isolated with SEC. In short, for EV analysis, 500 µl of serum was loaded onto the column (qEV original/70nm, IZON Science, USA), and eluted with dPBS. Four fractions of 500 µl (fractions 1-4) were collected after the void volume (2.7 ml) with an automated fraction collector (IZON Science, USA), combined and concentrated using ultrafiltration (Amicon Ultra, Merck KGaA, Germany). To dilute samples for interferometric reflectance imaging sensing (SP-IRIS), particle counts of EVs were measured by nanoparticle tracking analysis using ZetaView (Particle Metrix, Germany) and its corresponding software (version 8.05.12 SP2). Before measurements were taken, the accuracy of the ZetaView was verified using 100 nm polystyrene beads. Samples were diluted in 0.1 µm filtered dPBS to achieve a particle count in the range of 200–500 (1:5000–1:10000). Analyses were conducted in the scattered light mode with a laser wavelength of 488 nm. Next, the isolated EVs were analyzed with single particle SP-IRIS using an ExoView™ Plasma Tetraspanin kit and an ExoView™ R100 scanner (NanoView Biosciences, USA) according to the manufacturer's instructions. The samples were diluted to about 5 x10^9 particles /ml with the incubation buffer provided in the kit. All samples (40 µl of each) were added to the chip and incubated at room temperature for 16 h. The samples were then subjected to immune-fluorescence staining using fluorescently labelled antibodies (CD9/CD63/CD81, provided in the kit), washed, dried, and scanned. Data was analyzed using the NanoViewer analysis software version 3.0.

Density gradient ultracentrifugation

The third fraction (6 ml) of pooled serum samples was used for HDL particle isolation with density gradient ultracentrifugation. First, the APOB-containing particles were isolated using potassium bromide (KBr) -based density buffer (0.3184 g/ml KBr, PBS, 0.1% EDTA). Volume was set to 9 ml, and the serum was ultracentrifuged for 20 hours in a Ti 70.1 rotor (Beckman Coulter, IN, USA; 65000 rpm; g_{max} = 388024 x g) at a density of 1.063 g/ml. After this, the upper 2.25 ml fraction (i.e., the APOB-containing particles), and middle phase (4.5 ml) were collected from the top of the ultracentrifugation tube and stored at -80 °C. The bottom phase of 2.25 ml was collected, the density was set to 1.21 g/ml with solid KBr, and the volume was reset to 9 ml with isolation buffer. Next, the samples were ultracentrifuged in a Ti 70.1 rotor for 48 hours, after which the top 2.25 ml HDL particle-containing phase, was collected, and stored at -80 °C prior to further analysis.

Lipid extraction and protein isolation

Stored HDL was thawed on ice, after which the protein component was precipitated with methanol. The lipid content was extracted with sequential extraction with methanol, acetone, diethyl ether ethanol, and chloroform/methanol[63–66]. Combined supernatants containing the lipid proportion were

dried under nitrogen gas (N_2) flow, reconstituted with chloroform-methanol (1:2) mixture and stored in a glass vial at -20 °C until analysis. The combined protein-containing pellets were dried under N_2 flow, reconstituted with urea-thiourea buffer (7M urea, 2M thiourea, 0.2M ammonium bicarbonate, 4% CHAPS) and stored at -20 °C until analysis.

Lipid mass spectrometry

Before the mass spectrometry analysis, the sample solutions in chloroform/methanol (1:2 by vol) were spiked with a quantitative standard mixture (SPLASH, Avanti, Alabama, USA), and to enhance ionization and prevent adduct formation, 1% HN_3 was added just before the analysis. The mass spectra indicating all positively or negatively charged lipids, lipid precursors of the ions m/z 184 (LPCs, PCs and SMs), m/z 369 (CEs) and m/z 241 (phosphatidylinositols), and lipids assigned through neutral loss of amu 141 (phosphatidylethanolamines) and 87 (phosphatidylserines) were recorded by an Agilent 6410 Triple Quad LC-MS after infusing the sample solution with a syringe pump (flow rate 10 µl/min). The data were further analyzed with MassHunter Qualitative Analysis Navigator B.08.00 (Agilent Technologies, CA, USA) and LIMSA software[67].

Fatty acid gas chromatography

After removing solvents with N_2, aliquots of the extracted lipids were converted to FAMEs by heating in 1% methanolic H_2SO_4 with hexane as cosolvent at 95 °C for 120 min under N_2 atmosphere. After adding water, the FAMEs were extracted with hexane, dried with anhydrous Na_2SO_4, concentrated under N_2 flow and stored at -80 °C. The FA composition of the HDL particles was analyzed by injecting the FAME samples into a GC-2010 Plus gas chromatograph (Shimadzu Scientific Instruments, Japan) with a flame-ionization detector and integrating the resulting chromatographic peaks using a Shimadzu GC solution 2.42 software. Identification of the FAMEs was based on EI mass spectra recorded by a GCMS-QP2010 Ultra (Shimadzu Scientific Instruments) with a mass selective detector (MSD). Both systems were equipped with Zebron ZB-wax capillary columns (30 m, 0.25 mm ID and film thickness 0.25 µm; Phenomenex, CA, USA). The FA compositions were expressed as mol-% profiles.

Label-free HDL protein omics and bioinformatic data analysis

The protein samples were digested in Amicon Ultra 0.5 centrifugal filters using a modified FASP method, as described[68]. The peptides were cleaned using C18-reverse-phase ZipTip™ (Millipore, Merck KGaA). The dried peptide digest was re-suspended in 1% trifluoroacetic acid and sonicated in a water bath for 1 min before injection. Protein digests were analyzed using nano-LC-Thermo Q Exactive Plus. The peptides were separated by an Easy-nLC system (Thermo Scientific) equipped with a reverse-phase trapping column Acclaim PepMap™ 100 (C18, 75 µm × 20 mm, 3 µm particles, 100 Å; Thermo Scientific). The injected sample analytes were trapped at a flow rate of 2 µl min^{-1} in 100% of solution A (0.1 % formic acid). After trapping, the peptides were separated with a linear gradient of 120 min comprising 96 min from 3% to 30% of solution B (0.1% formic acid/80% acetonitrile), 7 min from 30% to 40% of solution B, and 4 min from 40% to 95% of solution B. Each sample run was followed by an empty run, which comprises a trap column flush with 16 µl of 80% acetonitrile to reduce the sample carryover from previous runs. LC-MS data acquisition was done with the mass spectrometer settings as follows: The resolution was set to 140,000 for MS scans, and 17,500 for the MS/MS scans. Full MS was acquired from 350 to 1400 m/z, and the 10 most abundant precursor ions were selected for fragmentation with 30 s dynamic exclusion time. Ions with 2+, 3+, and 4+ charges were selected for MS/MS analysis. Secondary ions were isolated with a window of 1.2 m/z. The MS

AGC target was set to 3 x 10^6 counts, whereas the MS/MS AGC target was set to 1 x 10^5. Dynamic exclusion was set with a duration of 20 s. The NCE collision energy step was set to 28 kJ mol^{-1}.

Following LC-MS/MS acquisition, for the relative quantification of proteins, the raw files were qualitatively analyzed by Proteome Discoverer (PD), version 2.4 (Thermo Scientific). The identification of proteins by PD was performed against the UniProt Human protein database (UniProt release 2020_12 downloaded on January 26th, 2021, with 20406 entries) using the built-in SEQUEST HT engine. The following parameters were used: 10 ppm and 0.02 Da were tolerance values set for MS and MS/MS, respectively. Trypsin was used as the digesting enzyme, and two missed cleavages were allowed. The carbamidomethylation of cysteines was set as a fixed modification, while the oxidation of methionine and deamidation of asparagine and glutamine were set as variable modifications. The false discovery rate was set to less than 0.01 and a peptide minimum length of six amino acids. Chromatograms were automatically aligned by the Progenesis QI for Proteomics™ (NonLinear Dynamics) software using the default values by following the wizard, and those that had an alignment score > 60% to the reference run were selected for further analysis. As a final filtering step, only proteins that were detected in at least two technical replicates of two samples in each menopausal group were accepted for further analysis.

LCAT activity assay

LCAT activity was measured from the serum samples of 10 premenopausal, 9 perimenopausal, and 9 postmenopausal women who were BMI-matched to the mean of the women used in earlier serum pools, i.e., to BMI about 25 kg/m^2. LCAT activity assay kit (Sigma-Aldrich MAK107, Merck) was used according to the manufacturer's instructions.

THP-1 macrophages and cholesterol efflux assay

The THP-1 monocyte line (TIB-202, ATCC, VI, USA) was maintained according to the provider's instructions. Briefly, monocytes were cultured in RPMI-1640 (Gibco, UK) with 10% heat-inactivated fetal bovine serum (FBS, Gibco) and 0.05 mM 2-mercaptoethanol (Sigma-Aldrich, Merck). For differentiating to macrophages, monocytes were seeded with 100 nM of phorbol 12-myristate 13-acetate (Sigma-Aldrich, Merck) into a 96-well tissue culture plate (60,000 cells/well, 100 µl/well) and incubated for 72 h. The cholesterol efflux assay was performed according to the kit instructions (Sigma-Aldrich MAK192, Merck) without FBS present. Macrophages were incubated with fluorescently labelled cholesterol for 1 h and then equilibrated overnight. After washing with FBS-free RPMI-1640, three concentrations of PRE-, PERI-, and POST-HDL samples (50, 125 and 200 µg/ml total HDL protein) with positive and negative controls were added to the cells and incubated for 4 h. At the end of the incubation, the amount of fluorescence of supernatant and solubilized cells was measured with a Glomax multi + detection system (Promega, WI, USA). The efflux capacity was calculated from the ratio of fluorescent intensity in the supernatant and the total fluorescent intensity from the supernatant and cell lysate. Cells were kept in a humidified CO_2 atmosphere at 37˚C during culturing, differentiation and efflux assay and passage number 6 was used in efflux assay.

Statistical Analyses, Data Processing, and Figures

Calculation of statistical significance was performed with IBM SPSS statistics (Version 26, IBM, USA). One-way ANOVA was used with Tukey's Honest Significant Difference test as a *post-hoc* to explore differences between multiple groups' means. For skewed variables indicated by histograms and Q-Q-plots, the Kruskal-Wallis test was used. For the LCAT activity test, the paired samples T-test was used

to analyze differences between groups. P values smaller or equal to 0.05 were considered significant. Because large correlations were assumed between lipid or protein species, multiple testing corrections were expected to give misleading results and were not done[69,70].

To investigate whether the three menopausal groups differ by some combination of multiple features, dimensionality reduction with Partial Least Squares Discriminant Analysis (PLS-DA) was performed with R package *mixOmics*[71]. As the protein and lipid data were already normalized, no further pre-processing steps were done. To detect correlations between proteins and lipids, omics integration was done with *mixOmics*. Correlation circles obtained from block sparse PLS-DA were plotted and corresponding Clustered Image Maps (CIM) were calculated. The CIM was re-plotted with a heatmap.2 function of R package *gplots* to control dendrogram ordering.

Fig. 1 was created with BioRender.com. Other figures (except Fig. 5) were plotted with the R package *ggplot2*. The data for the figures was processed using RStudio and R version 4.3.1.

Data availability

Datasets including the source data supporting our findings are shared either as supplementary tables or as source data files with this paper. The complete individual-level data is not publicly available due to privacy or ethical restrictions. Access to the data may be granted upon justification for research purposes taken that a request does not violate the consent provided by the study participants. Such requests should be addressed to the project leader (eija.k.laakkonen@jyu.fi) and will be evaluated with the board consisting of senior researchers involved in the ERMA study. The metadata of the ERMA study is publicly available (doi:10.17011/jyx/dataset/83491).

Code availability

The main code used to conduct this study is available on GitHub at LaakkonenLab/MATCH (github.com).

Acknowledgements

This study was funded by grants from the Academy of Finland (grant numbers 33028, 309504, 314181, and 335249 to E.K.L). We acknowledge the following core units of the University of Helsinki: the EV Core for SEC and SP-IRIS analyses, the HiLIPID unit of the HiLIFE for lipidomic analyses and the Meilahti Clinical Proteomics unit of the HiLIFE for proteomic analyses. We thank the staff at the Faculty of Sport and Health Sciences of the University of Jyväskylä for their invaluable assistance with data collection. We also thank the women who participated in the ERMA study for donating their time and effort.

Author contributions

E.K.L. is the PI of the ERMA study and together with M.L. designed and supervised the current study. E.K.L. provided funding for the study. S.L. did a majority of the laboratory work including HDL particle isolations, lipid and protein extractions, ESI-MS and LCAT assays. S.L. analysed lipidomics datasets concerning lipid classes and lipid species. H.R. and R.K. performed GC-FID and GC-MSD analyses of fatty acids. R.S. did protein LC-MS and analysis of the data which M.La. supervised. S.L. did data curation for lipidomic and proteomic datasets. E.L. did cholesterol efflux assays. M.P. and P.S. were responsible for the EV isolations and analysis. S.L. constructed the Data Source files and did the statistics and visualization based on them. T-M.K. performed the bioinformatic analyses for Figure 7 and polished the figures using R packages. S.L. wrote the original draft of the manuscript. T-M.K., M.L. and E.K.L. contributed to the editing of the manuscript. All co-authors have participated in the interpretation of the results and critically commented on the manuscript during the writing process. E.K.L. prepared the final version of the manuscript, which all the co-authors approved.

Competing interests

The authors declare no competing interests.

References

1. Wang, Q. *et al.* Metabolic characterization of menopause: cross-sectional and longitudinal evidence. *BMC Med.* **16**, 17 (2018).
2. Auro, K. *et al.* A metabolic view on menopause and ageing. *Nat. Commun.* **5**, 4708 (2014).
3. Karppinen, J. E. *et al.* Menopause modulates the circulating metabolome: evidence from a prospective cohort study. *Eur. J. Prev. Cardiol.* **29**, 1448–1459 (2022).
4. El Khoudary, S. R. *et al.* HDL (High-Density Lipoprotein) Subclasses, Lipid Content, and Function Trajectories Across the Menopause Transition: SWAN-HDL Study. *Arterioscler. Thromb. Vasc. Biol.* **41**, 951–961 (2021).
5. Hyvärinen, M. *et al.* Metabolic health, menopause, and physical activity—a 4-year follow-up study. *Int. J. Obes.* **46**, 544–554 (2021).
6. Camont, L., Chapman, M. J. & Kontush, A. Biological activities of HDL subpopulations and their relevance to cardiovascular disease. *Trends Mol. Med.* **17**, 594–603 (2011).
7. Kontush, A., Lhomme, M. & Chapman, M. J. Unraveling the complexities of the HDL lipidome. *J. Lipid Res.* **54**, 2950–2963 (2013).
8. Davidson, W. S., Shah, A. S., Sexmith, H. & Gordon, S. M. The HDL Proteome Watch: Compilation of studies leads to new insights on HDL function. *Biochim. Biophys. Acta BBA - Mol. Cell Biol. Lipids* **1867**, 159072 (2022).
9. Von Eckardstein, A., Nordestgaard, B. G., Remaley, A. T. & Catapano, A. L. High-density lipoprotein revisited: biological functions and clinical relevance. *Eur. Heart J.* **44**, 1394–1407 (2023).
10. Rohatgi, A., Westerterp, M., von Eckardstein, A., Remaley, A. & Rye, K.-A. HDL in the 21st Century: A Multifunctional Roadmap for Future HDL Research. *Circulation* **143**, 2293–2309 (2021).
11. Rached, F. H., Chapman, M. J. & Kontush, A. HDL particle subpopulations: Focus on biological function. *BioFactors* **41**, 67–77 (2015).
12. Mehta, N. *et al.* The evolving role of cholesteryl ester transfer protein inhibition beyond cardiovascular disease. *Pharmacol. Res.* **197**, 106972 (2023).
13. Jonas, A. Lecithin-cholesterol acyltransferase in the metabolism of high-density lipoproteins. *Biochim. Biophys. Acta* **1084**, 205–220 (1991).
14. Kovanen, V. *et al.* Design and protocol of Estrogenic Regulation of Muscle Apoptosis (ERMA) study with 47 to 55-year-old women's cohort: novel results show menopause-related differences in blood count. *Menopause* **25**, 1020 (2018).
15. Ala-Korpela, M., Zhao, S., Järvelin, M.-R., Mäkinen, V.-P. & Ohukainen, P. Apt interpretation of comprehensive lipoprotein data in large-scale epidemiology: disclosure of fundamental structural and metabolic relationships. *Int. J. Epidemiol.* **51**, 996–1011 (2022).
16. Kettunen, J. *et al.* Lipoprotein signatures of cholesteryl ester transfer protein and HMG-CoA reductase inhibition. *PLOS Biol.* **17**, e3000572 (2019).
17. Rainwater, D. L., Ludwig, M. J., Haffner, S. M. & VandeBerg, J. L. Lipid and Lipoprotein Factors Associated With Variation in Lp(a) Density. *Arterioscler. Thromb. Vasc. Biol.* **15**, 313–319 (1995).
18. Simonsen, J. B. What Are We Looking At? Extracellular Vesicles, Lipoproteins, or Both? *Circ. Res.* **121**, 920–922 (2017).
19. Nieuwland, R. & Siljander, P. R.-M. A beginner's guide to study extracellular vesicles in human blood plasma and serum. *J Extracell Vesicles* **In Press**, (2023).
20. Malajczuk, C. J., Gandhi, N. S. & Mancera, R. L. Structure and intermolecular interactions in spheroidal high-density lipoprotein subpopulations. *J. Struct. Biol. X* **5**, 100042 (2021).
21. González, I., Cao, K.-A. L., Davis, M. J. & Déjean, S. Visualising associations between paired 'omics' data sets. *BioData Min.* **5**, 19 (2012).

22. Davit-Spraul, A. *et al.* Cholesterol efflux from Fu5AH cells to the serum of patients with Alagille syndrome: importance of the HDL-phospholipids/free cholesterol ratio and of the HDL size distribution. *J. Lipid Res.* **40**, 328–335 (1999).
23. Barter, P. J. *et al.* Cholesteryl ester transfer protein: a novel target for raising HDL and inhibiting atherosclerosis. *Arterioscler. Thromb. Vasc. Biol.* **23**, 160–167 (2003).
24. Johnson, W. J., Mahlberg, F. H., Rothblat, G. H. & Phillips, M. C. Cholesterol transport between cells and high-density lipoproteins. *Biochim. Biophys. Acta BBA - Lipids Lipid Metab.* **1085**, 273–298 (1991).
25. Hodson, L., Skeaff, C. M. & Fielding, B. A. Fatty acid composition of adipose tissue and blood in humans and its use as a biomarker of dietary intake. *Prog. Lipid Res.* **47**, 348–380 (2008).
26. Lommi, J. I. *et al.* High-density lipoproteins (HDL) are present in stenotic aortic valves and may interfere with the mechanisms of valvular calcification. *Atherosclerosis* **219**, 538–544 (2011).
27. Davidson, W. S. *et al.* Proteomic analysis of defined hdl subpopulations reveals particle-specific protein clusters: Relevance to antioxidative function. *Arterioscler. Thromb. Vasc. Biol.* **29**, 870–876 (2009).
28. Guan, C.-L. *et al.* Is elevated triglyceride/high-density lipoprotein cholesterol ratio associated with poor prognosis of coronary heart disease? A meta-analysis of prospective studies. *Medicine (Baltimore)* **101**, e31123 (2022).
29. Tangney, C. C., Mosca, L. J., Otvos, J. D. & Rosenson, R. S. Oral 17β-estradiol and medroxyprogesterone acetate therapy in postmenopausal women increases HDL particle size. *Atherosclerosis* **155**, 425–430 (2001).
30. Piperi, C., Kalofoutis, C., Papapanagiotou, A., Skenderi, C. & Kalofoutis, A. Comparative analysis of oestrogen and raloxifene effects on the phospholipid composition of high density lipoproteins in healthy postmenopausal women. *J. Obstet. Gynaecol.* **24**, 52–57 (2004).
31. Brown, M. L. *et al.* Molecular basis of lipid transfer protein deficiency in a family with increased high-density lipoproteins. *Nature* **342**, 448–451 (1989).
32. Barter, P. J. *et al.* Cholesteryl Ester Transfer Protein. *Arterioscler. Thromb. Vasc. Biol.* **23**, 160–167 (2003).
33. Rashid, S. *et al.* Elevated cholesteryl ester transfer protein (CETP) activity, a major determinant of the atherogenic dyslipidemia, and atherosclerotic cardiovascular disease in South Asians. *Eur. J. Prev. Cardiol.* **22**, 468–477 (2015).
34. Skeggs, J. W. & Morton, R. E. LDL and HDL enriched in triglyceride promote abnormal cholesterol transport. *J. Lipid Res.* **43**, 1264–1274 (2002).
35. Villard, E. F. *et al.* Elevated CETP Activity Improves Plasma Cholesterol Efflux Capacity From Human Macrophages in Women. *Arterioscler. Thromb. Vasc. Biol.* **32**, 2341–2349 (2012).
36. Johnson, W. J. *et al.* The bidirectional flux of cholesterol between cells and lipoproteins. Effects of phospholipid depletion of high density lipoprotein. *J. Biol. Chem.* **261**, 5766–5776 (1986).
37. Badeau, R. M., Metso, J., Wähälä, K., Tikkanen, M. J. & Jauhiainen, M. Human macrophage cholesterol efflux potential is enhanced by HDL-associated 17β-estradiol fatty acyl esters. *J. Steroid Biochem. Mol. Biol.* **116**, 44–49 (2009).
38. Liu, C., Gaudet, D. & Miller, Y. I. Deficient Cholesterol Esterification in Plasma of apoc2 Knockout Zebrafish and Familial Chylomicronemia Patients. *PLOS ONE* **12**, e0169939 (2017).
39. Amaya-Montoya, M. *et al.* ApoE and apoC-III-defined HDL subtypes: a descriptive study of their lecithin cholesterol acyl transferase and cholesteryl ester transfer protein content and activity. *Lipids Health Dis.* **19**, 106 (2020).
40. Tabassum, R. *et al.* Lipidome- and Genome-Wide Study to Understand Sex Differences in Circulatory Lipids. *J. Am. Heart Assoc.* **11**, e027103 (2022).
41. Ekroos, K. *et al.* Lipid-based biomarkers for CVD, COPD, and aging – A translational perspective. *Prog. Lipid Res.* **78**, 101030 (2020).
42. Cheng, S. *et al.* Distinct metabolomic signatures are associated with longevity in humans. *Nat. Commun.* **6**, 6791 (2015).

43. Jenkins, B. J. *et al.* Odd Chain Fatty Acids; New Insights of the Relationship Between the Gut Microbiota, Dietary Intake, Biosynthesis and Glucose Intolerance. *Sci. Rep.* **7**, 44845 (2017).
44. Sergeant, S., Rahbar, E. & Chilton, F. H. Gamma-linolenic acid, Dihommo-gamma linolenic, Eicosanoids and Inflammatory Processes. *Eur. J. Pharmacol.* **785**, 77–86 (2016).
45. Sheppe, A. E. F. & Edelmann, M. J. Roles of Eicosanoids in Regulating Inflammation and Neutrophil Migration as an Innate Host Response to Bacterial Infections. *Infect. Immun.* **89**, e00095-21 (2021).
46. Zhu, C. *et al.* The HDL lipidome is widely remodeled by fast food versus Mediterranean diet in 4 days. *Metabolomics* **15**, 114 (2019).
47. Melchior, J. T. *et al.* Apolipoprotein A-I modulates HDL particle size in the absence of apolipoprotein A-II. *J. Lipid Res.* **62**, 100099 (2021).
48. Applebaum-Bowden, D. *et al.* Lipoprotein, apolipoprotein, and lipolytic enzyme changes following estrogen administration in postmenopausal women. *J. Lipid Res.* **30**, 1895–1906 (1989).
49. Li, J., Sun, H., Wang, Y., Liu, J. & Wang, G. Apolipoprotein C3 is negatively associated with estrogen and mediates the protective effect of estrogen on hypertriglyceridemia in obese adults. *Lipids Health Dis.* **22**, 29 (2023).
50. Nishida, H. I. *et al.* Nature of the enhancement of lecithin-cholesterol acyltransferase reaction by various apolipoproteins. *J. Biol. Chem.* **261**, 12028–12035 (1986).
51. Lund-Katz, S. & Phillips, M. C. High Density Lipoprotein Structure–Function and Role in Reverse Cholesterol Transport. *Subcell. Biochem.* **51**, 183–227 (2010).
52. Rye, K.-A., Wee, K., Curtiss, L. K., Bonnet, D. J. & Barter, P. J. Apolipoprotein A-II Inhibits High Density Lipoprotein Remodeling and Lipid-poor Apolipoprotein A-I Formation *. *J. Biol. Chem.* **278**, 22530–22536 (2003).
53. Larsson, M., Vorrsjö, E., Talmud, P., Lookene, A. & Olivecrona, G. Apolipoproteins C-I and C-III Inhibit Lipoprotein Lipase Activity by Displacement of the Enzyme from Lipid Droplets. *J. Biol. Chem.* **288**, 33997–34008 (2013).
54. Pillois, X. *et al.* Constitutive inhibition of plasma CETP by apolipoprotein C1 is blunted in dyslipidemic patients with coronary artery disease. *J. Lipid Res.* **53**, 1200–1209 (2012).
55. Luo, M. *et al.* ApoCIII enrichment in HDL impairs HDL-mediated cholesterol efflux capacity. *Sci. Rep.* **7**, 2312 (2017).
56. Chernyaeva, L. *et al.* Reduced binding of apoE4 to complement factor H promotes amyloid-β oligomerization and neuroinflammation. *EMBO Rep.* e56467 (2023) doi:10.15252/embr.202256467.
57. Gaudreault, N. *et al.* ApoE Suppresses Atherosclerosis by Reducing Lipid Accumulation in Circulating Monocytes and the Expression of Inflammatory Molecules on Monocytes and Vascular Endothelium. *Arterioscler. Thromb. Vasc. Biol.* **32**, 264 (2012).
58. de Beer, M. C. *et al.* Characterization of constitutive human serum amyloid A protein (SAA4) as an apolipoprotein. *J. Lipid Res.* **36**, 526–534 (1995).
59. Fernández, J. A., Deguchi, H., Elias, D. J. & Griffin, J. H. Serum amyloid A4 is a procoagulant apolipoprotein that it is elevated in venous thrombosis patients. *Res. Pract. Thromb. Haemost.* **4**, 217–223 (2019).
60. Webb, N. R. High-Density Lipoproteins and Serum Amyloid A (SAA). *Curr. Atheroscler. Rep.* **23**, 7 (2021).
61. Holzer, M. *et al.* HDL Isolated by Immunoaffinity, Ultracentrifugation, or Precipitation is Compositionally and Functionally Distinct. *J. Lipid Res.* **63**, 100307 (2022).
62. Soininen, P., Kangas, A. J., Würtz, P., Suna, T. & Ala-Korpela, M. Quantitative Serum Nuclear Magnetic Resonance Metabolomics in Cardiovascular Epidemiology and Genetics. *Circ. Cardiovasc. Genet.* **8**, 192–206 (2015).

63. Veit, M., Ponimaskin, E. & Schmidt, M. F. G. Analysis of S-Acylation of Proteins. in *Post-translational Modifications of Proteins: Tools for Functional Proteomics* (ed. Kannicht, C.) 163–182 (Humana Press, 2008). doi:10.1007/978-1-60327-084-7_12.
64. Bizzozero, O. A. Chemical analysis of acylation sites and species. *Methods Enzymol.* **250**, 361–379 (1995).
65. Muszbek, L., Haramura, G., Cluette-Brown, J. E., Van Cott, E. M. & Laposata, M. The pool of fatty acids covalently bound to platelet proteins by thioester linkages can be altered by exogenously supplied fatty acids. *Lipids* **34 Suppl**, S331-337 (1999).
66. Olson, E. N., Towler, D. A. & Glaser, L. Specificity of fatty acid acylation of cellular proteins. *J. Biol. Chem.* **260**, 3784–3790 (1985).
67. Haimi, P., Uphoff, A., Hermansson, M. & Somerharju, P. Software Tools for Analysis of Mass Spectrometric Lipidome Data. *Anal. Chem.* **78**, 8324–8331 (2006).
68. Scifo, E. *et al.* Quantitative analysis of PPT1 interactome in human neuroblastoma cells. *Data Brief* **4**, 207–216 (2015).
69. Rothman, K. J. Six Persistent Research Misconceptions. *J. Gen. Intern. Med.* **29**, 1060–1064 (2014).
70. García-Pérez, M. A. Use and misuse of corrections for multiple testing. *Methods Psychol.* **8**, 100120 (2023).
71. Rohart, F., Gautier, B., Singh, A. & Lê Cao, K.-A. mixOmics: An R package for 'omics feature selection and multiple data integration. *PLOS Comput. Biol.* **13**, e1005752 (2017).

Tables

Table 1. Characteristics of the menopausal groups.

	PRE	**PERI**	**POST**	***P* for trend**
n (individuals/pools)	72/12	72/12	72/12	
Age	50.7 (0.8)	50.8 (0.9)	52.4 (0.6)	<0.001
Diet quality score	6.1 (1.1)	5.4 (0.9)	5.9 (0.9)	0.247
Leisure-time physical activity (MET-h/d)	4.5 (1.3)	4.1 (1.0)	3.9 (1.3)	0.492
BMI (kg/m^2)	25.5 (0.4)	25.6 (0.5)	25.0 (0.5)	0.043
Waist circumference (cm)	82.4 (2.4)	83.8 (2.6)	82.6 (1.7)	0.269
Systolic blood pressure (mmHg)	130.7 (5.3)	134.7 (7.7)	134.3 (5.9)	0.257
Diastolic blood pressure (mmHg)	83.5 (3.8)	85.7 (3.6)	85.9 (2.3)	0.141
Total cholesterol (mmol/l)	5.1 (0.4)	5.2 (0.5)	5.7 (0.4)	0.004
LDL-C (mmol/l)	2.9 (0.4)	3.1 (0.4)	3.4 (0.3)	0.004
HDL-C (mmol/l)	1.8 (0.1)	1.6 (0.1)	1.9 (0.2)	<0.001
TG (mmol/l)	1.0 (0.1)	1.1 (0.2)	1.0 (0.2)	0.527
Glucose (mmol/l)	5.2 (0.2)	5.2 (0.1)	5.0 (0.1)	0.004
Insulin (pmol/l)	44.3 (15.7)	51.9 (24.2)	49.8 (10.5)	0.567
Cortisol (nmol/l)	379.5 (48.1)	377.8 (37.0)	396.4 (40.7)	0.495
Estradiol (nmol/l)	0.7 (0.3)	0.4 (0.2)	0.1 (0.0)	<0.001
FSH (IU/l)	6.1 (2.1)	20.5 (10.5)	92.4 (25.5)	<0.001
SHBG (nmol/l)	65.4 (11.9)	62.9 (13.3)	51.5 (8.4)	0.006

Values are mean (standard deviation). abbreviations: BMI body mass index, LDL-C low-density cholesterol, HDL-C high-density cholesterol, TG triacylglycerol, FSH follicle stimulating hormone, SHBG sex hormone-binding globulin.

Figures

Fig. 1

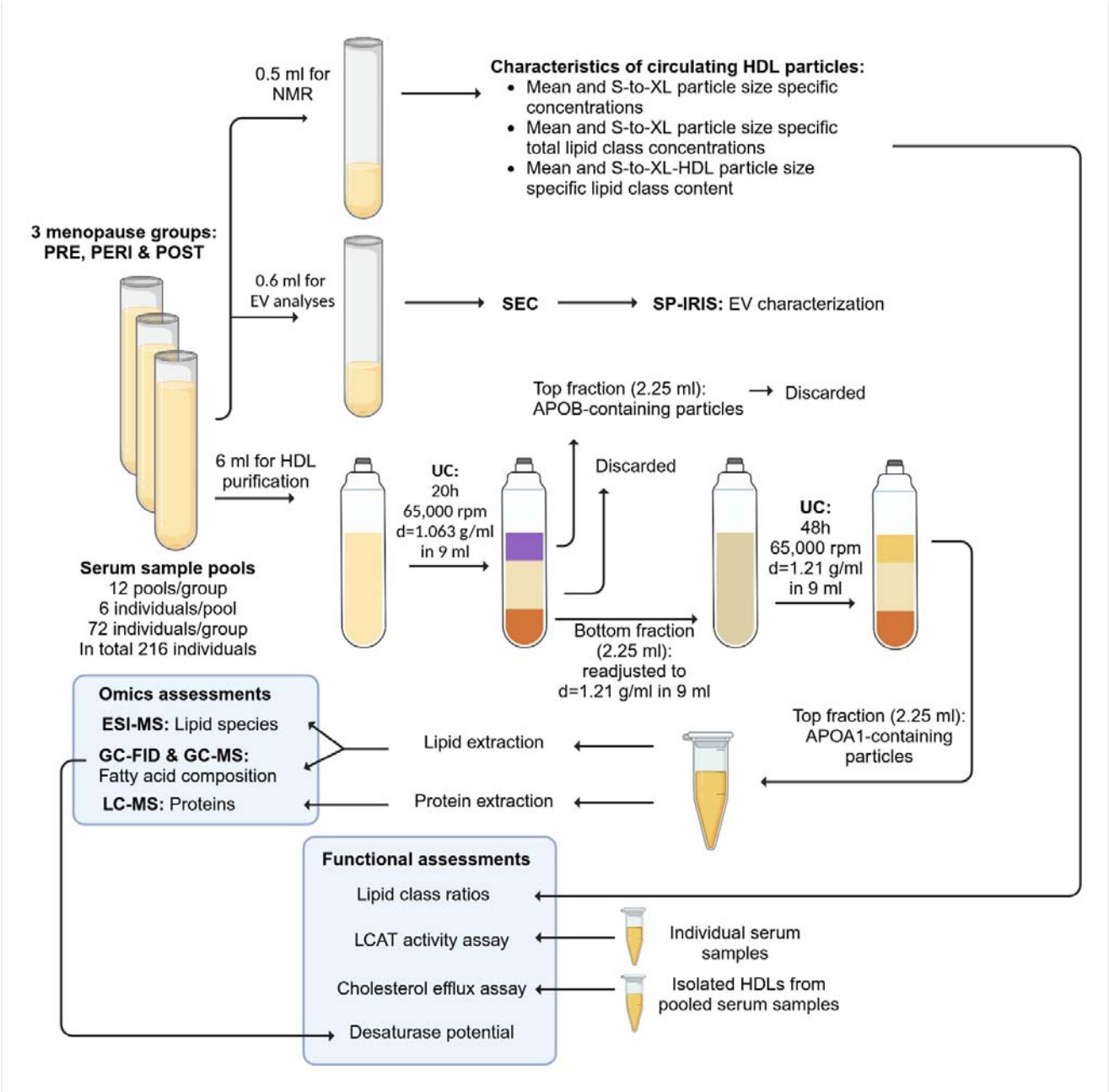

Fig. 1. Schematic of the study design and sample workflow.

Abbreviations: PRE, premenopausal, PERI, perimenopausal, POST, postmenopausal, NMR, nuclear magnetic resonance, HDL, high-density lipoprotein particle, EV, extracellular vesicle, SEC, size exclusion chromatography, SP-IRIS, single particle interferometric reflectance imaging sensing, UC, ultracentrifuge, APOB, apolipoprotein B, APOA1, apolipoprotein A1. ESI-MS, electrospray ionization-mass spectrometry, GC-FID, gas chromatography with flame ionization detector, GC-MS, gas chromatography-mass spectrometry, LC-MS, liquid chromatography-tandem mass spectrometry.

Fig. 2

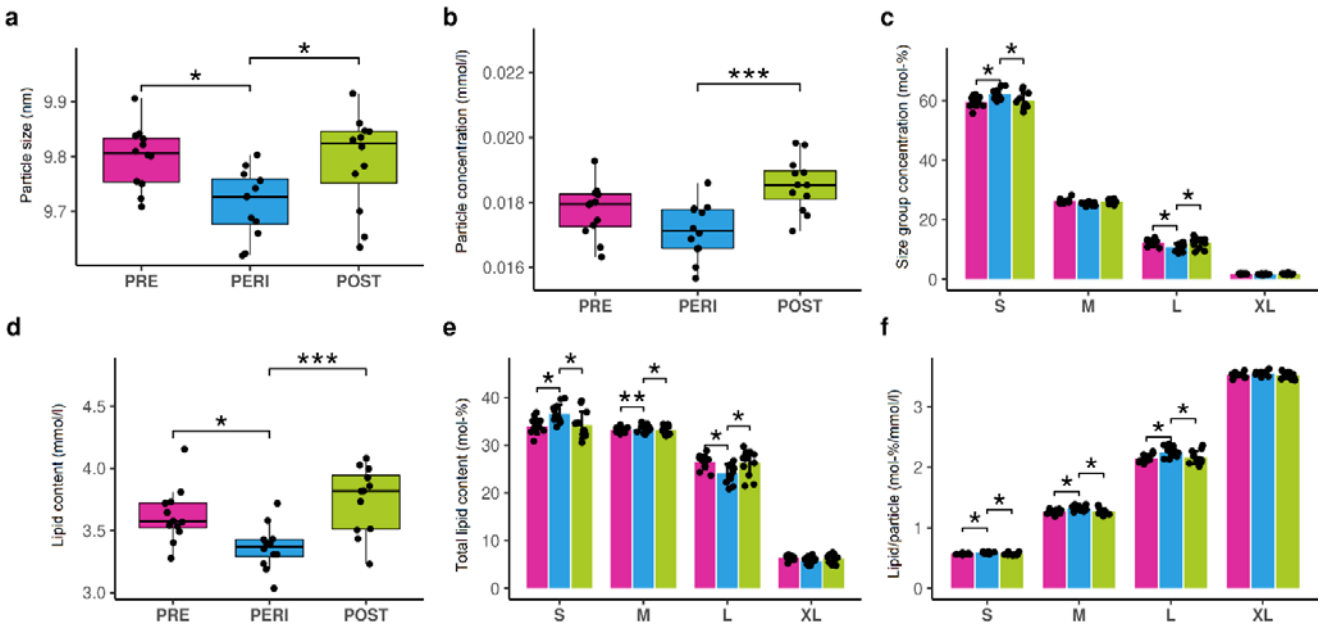

Fig. 2. **Physical properties of HDL particles measured with nuclear magnetic resonance spectroscopy.** **a** Total HDL particle sizes in menopausal groups (nm). **b** Total HDL particle concentration in serum (mmol/l). **c** Particle concentrations of HDL size groups (mol-%). **d** Total lipid content of HDL particles (mmol/l). **e** Total lipid content in the HDL particle size groups (mol-%). **f** Lipid per particle ratios in HDL particle size groups (mol-%/mmol/l). Statistical significance * < 0.05, **<0.01, ***<0.001. Abbreviations: PRE premenopause, PERI perimenopause, POST postmenopause, HDL high-density lipoprotein.

Fig. 3

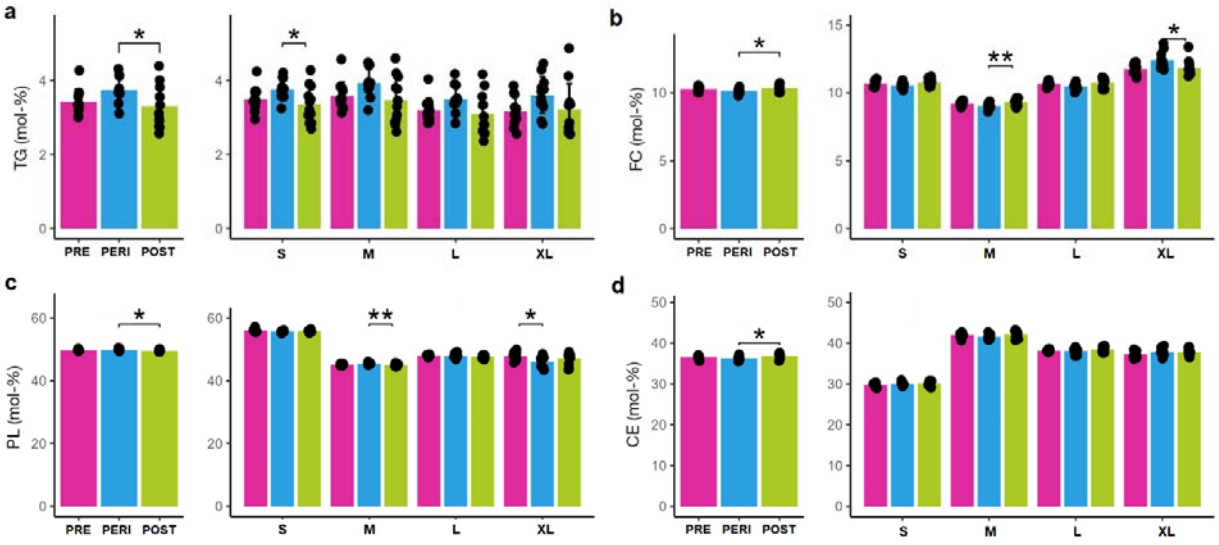

Fig. 3. The nuclear magnetic resonance analysis of the major lipid classes of menopausal women's HDL particles. Proportions of lipid classes are expressed in mol-%. **a** Mean and size-specific triacylglycerol (TG) content of HDL particles. **b**) Mean and size-specific unesterified cholesterol (FC) content of HDL particles. **c** Mean and size-specific phospholipid (PL) content of HDL particles. **d** Mean and size-specific cholesteryl esters (CE) content of HDL particles. Statistical significance * < 0.05, **<0.01. Abbreviations: PRE premenopause, PERI perimenopause, POST postmenopause, HDL high-density lipoprotein.

Fig. 4

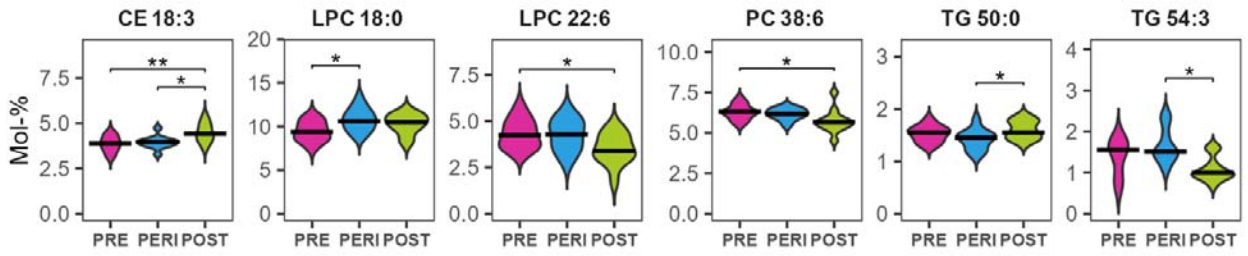

Fig. 4. HDL lipid species with significant differences between menopausal groups. Lipids were extracted from ultracentrifugally isolated HDL and analyzed with ESI-MS. Of all lipid species representing lipid classes CE, LPC, PC, SM and TG, only six were observed to have statistically significant differences in their relative concentration between menopausal groups. Statistical significance * < 0.05, **<0.01. Abbreviations: PRE premenopause, PERI perimenopause, POST postmenopause, CE cholesteryl ester, LPC lysophosphatidylcholine, PC phosphatidylcholine, SM sphingomyelin, TG triacylglycerol.

Fig. 5

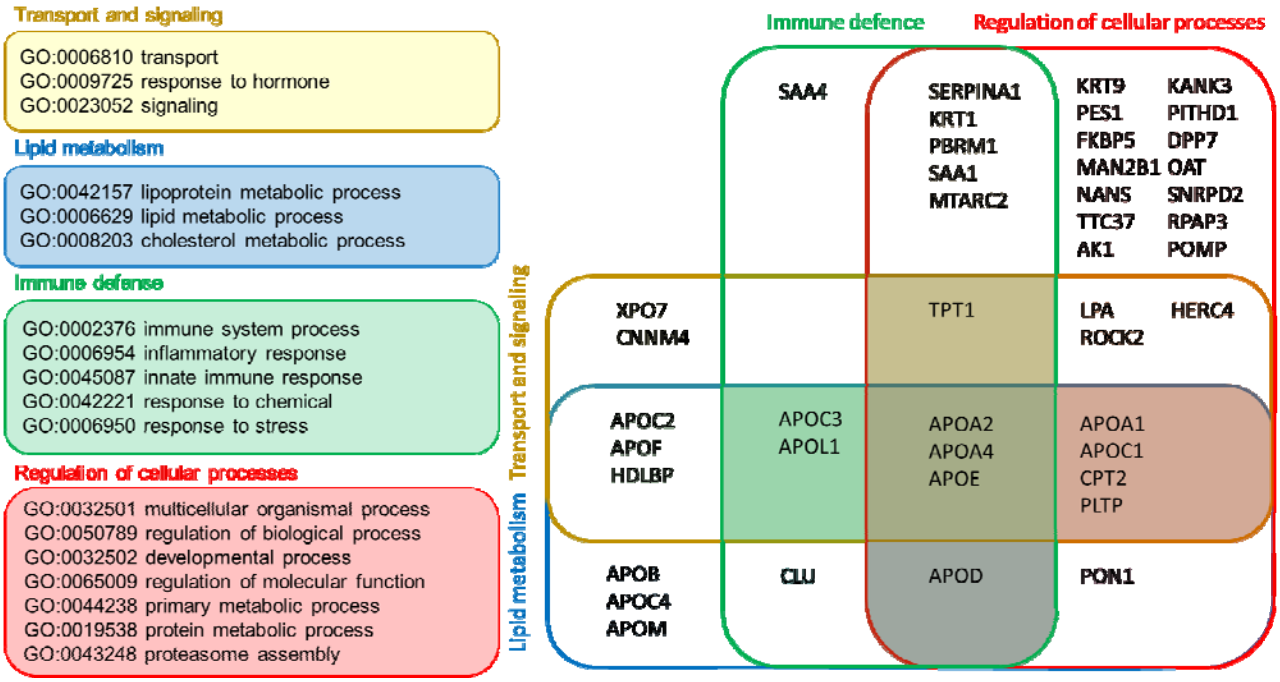

Fig. 5. The quantified HDL proteins are associated with four main categories of Gene Ontology. Of the 728 observed HDL proteins, the figure presents the 44 proteins that met the robust criteria allowing quantification, i.e., a protein needed to be present in at least two out of three technical replicates and simultaneously in two out of twelve sample pools per menopausal group. The functional classification of the HDL proteins is shown in the Venn diagram (right panel), while GO subcategories and corresponding GO identifiers are listed on the left panel.

Fig. 6

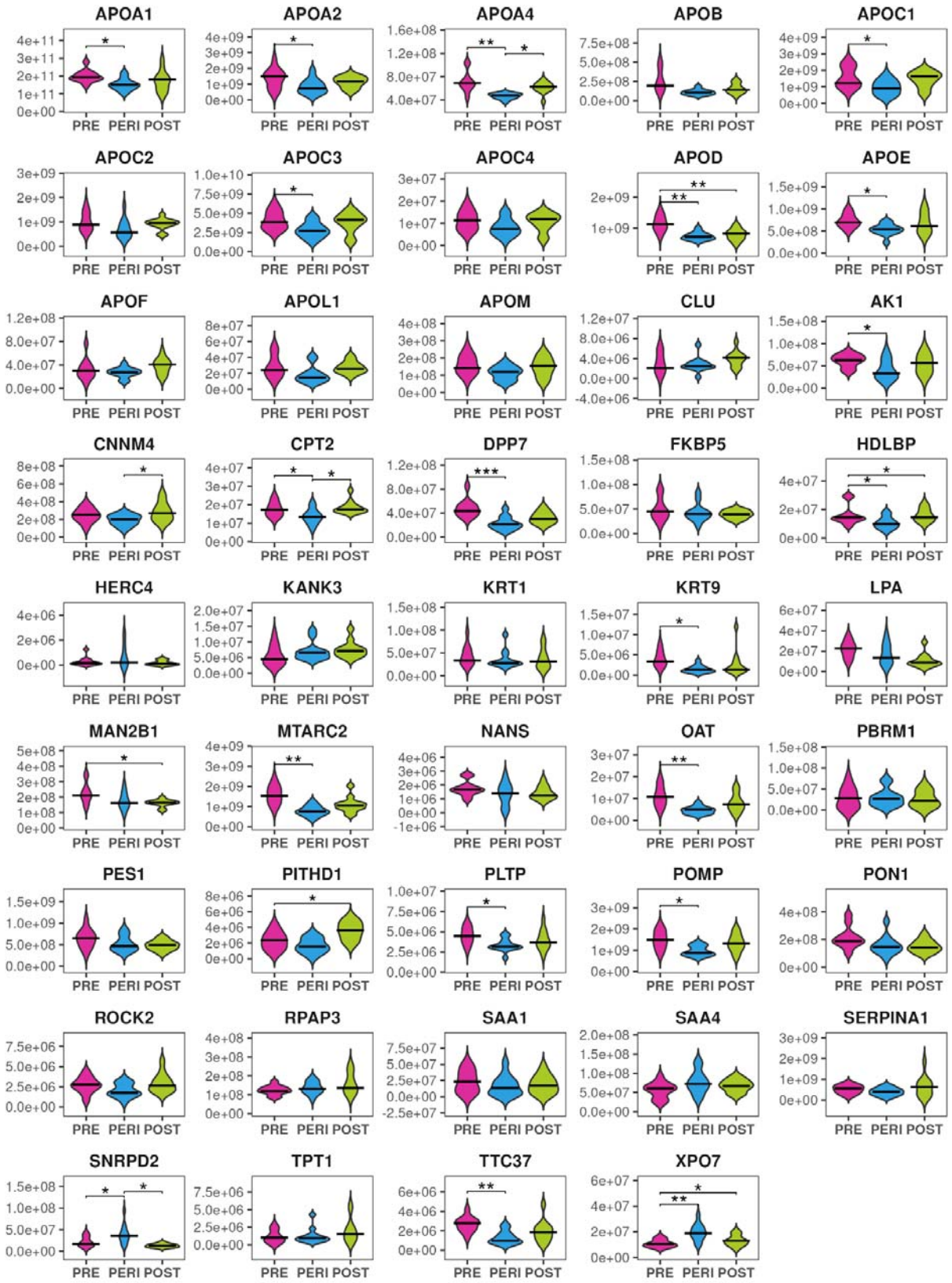

Fig. 6. Violin plots of HDL proteins normalized to HDL particle count. All protein abundances were measured with LC-MS method from the isolated HDL particles. HDL particle count was with NMR. Statistical significance * < 0.05, **<0.01, ***<0.001. Abbreviations: PRE premenopause, PERI perimenopause, POST postmenopause, HDL high density lipoprotein, LC-MS liquid chromatography mass spectrometry, NMR nuclear magnetic resonance.

Fig. 7

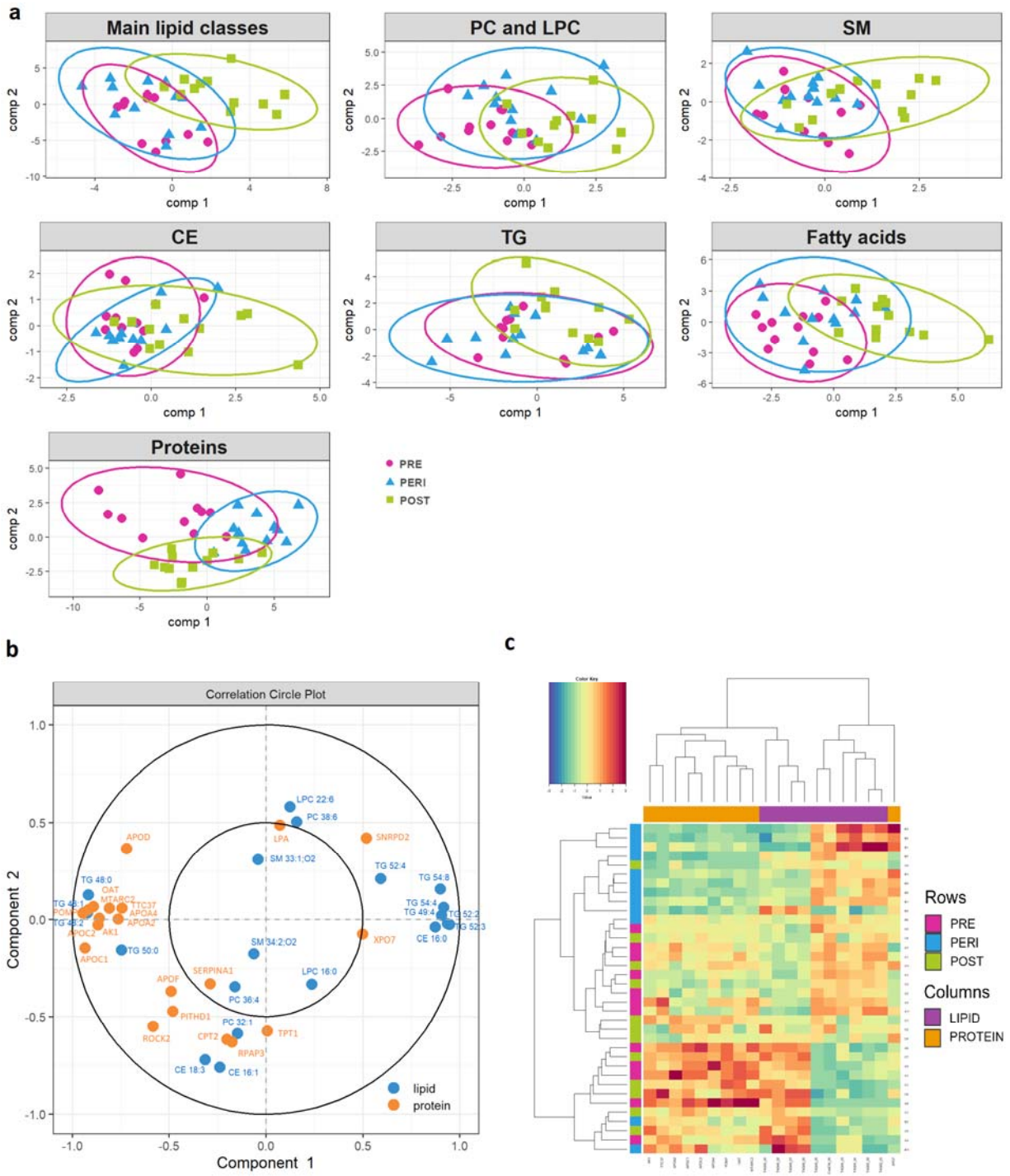

Fig 7. Multi-omics analyses of HDL in three menopausal statuses. a PLS discriminant analysis scores plots for fatty acids, lipid classes, and proteins. Main lipid classes, PC and LPC, SM, CE and TG, as well as FAs were analyzed with non-targeted mass spectrometry. Quantified protein profiles were assessed with un-targeted LC-MS/MS. Circles denote a 95% confidence interval. **b** Unsupervised correlation circle plot of lipid species and proteins. No correlation cut-off was applied. **c** Heat map of lipids and proteins. Abbreviations: PRE premenopause, PERI perimenopause, POST postmenopause, PC phosphatidylcholine, LPC lysophosphatidylcholine, SM sphingomyelin, CE cholesteryl ester, TG triacylglycerol.

Fig. 8

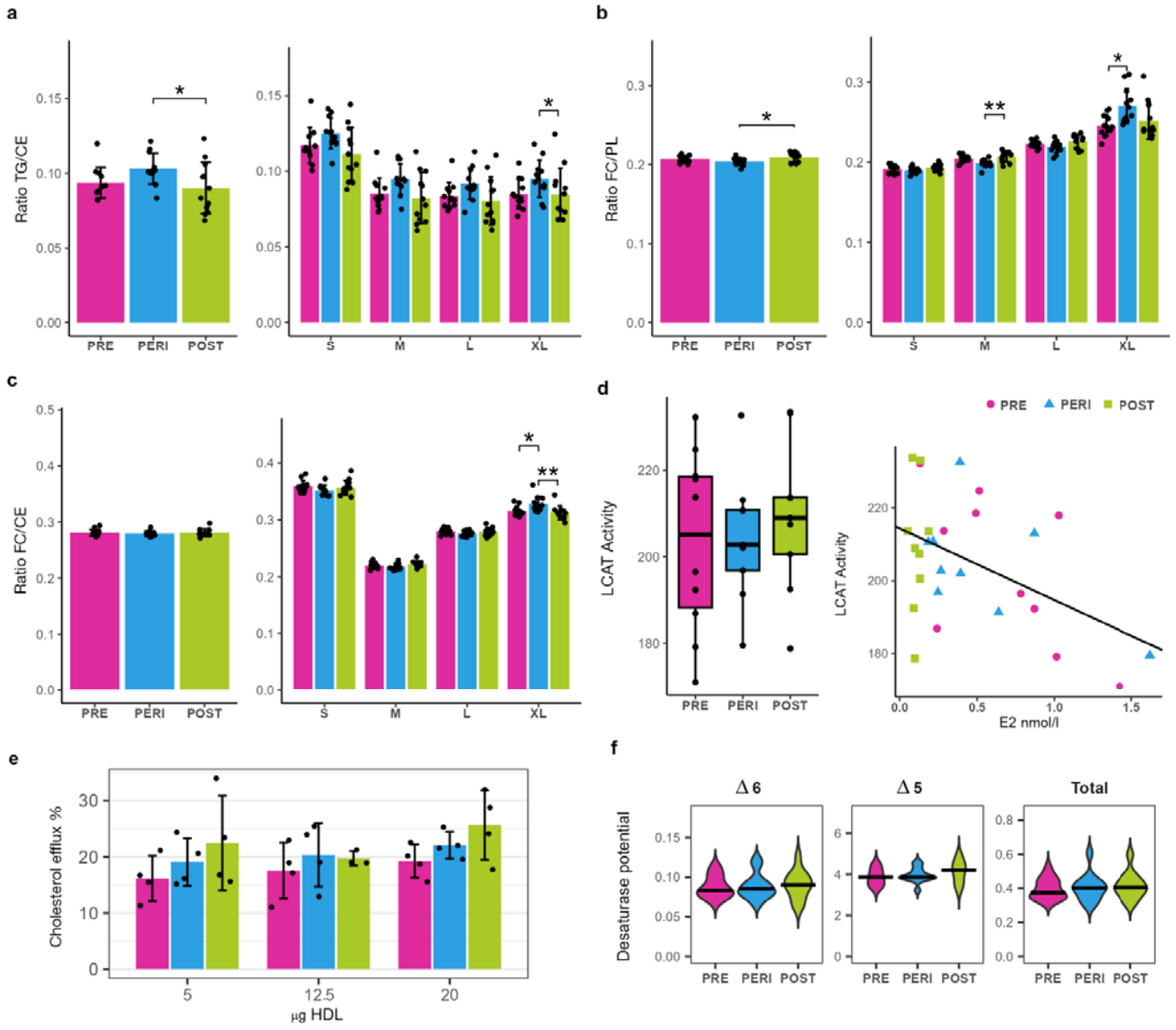

Fig. 8. Functional assessments of the HDL across menopausal stages. a Ratio of lipid classes TG/CE in total serum HDL and in HDL size groups. **b** Ratio of lipid classes FC/PL in total serum HDL and in HDL size groups. **c** Ratio of lipid classes FC/CE in total serum HDL and in HDL size groups. All lipid class ratios were calculated from lipid classes measured with NMR. **d** LCAT activity assay with serum samples representing PRE (n = 10), PERI (n = 9) and POST (n = 9) women. **e** Cholesterol efflux assay with 5 µg, 12.5 µg and 20 µg of purified HDL originating from the pooled serum samples of PRE, PERI and POST women. **f** Computational desaturase potentials. Δ6 desaturase potential was calculated with formula (18:3n-6 + 20:3n-6)/18:2n-6, Δ5 desaturase potential was calculated with formula (20:4n-6 + 22:4n-6)/20:3n-6, and total desaturase potential was calculated with formula (18:3n-6 + 20:3n-6 + 20:4n-6+22:4n-6 + 22:5n-6)/18:2n-6. Desaturase potentials were calculated from fatty acid molar percentages quantified by GC-FID and structures verified by GC-MS. Statistical significance * < 0.05, **<0.01. Abbreviations: PRE premenopause, PERI perimenopause, POST postmenopause, LCAT lecithin:cholesterol acyltransferase, E2 17β-estradiol, HDL high-density lipoprotein, TG triacylglycerol, CE cholesteryl ester, FC unesterified free cholesterol, PL phospholipids, NMR nuclear magnetic resonance, GC-FID gas chromatography with flame ionization detector, GC-MS gas chromatography mass spectrometry.